Observation of conical electron distributions over Martian crustal magnetic fields

Demet Ulusen,[1] David A. Brain,[1] and David L. Mitchell[1]

Received 15 October 2010; revised 24 March 2011; accepted 5 April 2011; published 15 July 2011.

[1] Electron angular distributions similar to bidirectional electron conics (BECs) near Earth's auroral regions have been previously reported at Mars. They are almost always symmetric about 90° pitch angle, having peaks between 35°–70° and 110°–145°. Signatures of Martian BECs are clearly observable from ~90 eV to ~640 eV and they are mainly observed in darkness (60% of 150,000 conic events identified globally). Statistical analysis shows that BECs mostly occur on horizontal magnetic field lines over moderate crustal fields (~15 nT). They are surrounded by regions containing electrons with trapped/mirroring pitch angle distributions, which suggests that BECs form on closed field lines. The energy spectra of the conics exhibit substantial decreases in all energy levels in relation to neighboring regions, which mostly have access to the Martian magnetotail or magnetosheath. Upstream conditions (draped IMF direction, solar wind pressure, and EUV flux) do not affect the observation of the events. Therefore stability inferred from observations of similar BECs over the same geographical locations suggests that the driving conditions resulting in their formation operate on the crustal fields. We propose that conical electron distributions may be generated by merging of neighboring open crustal magnetic field lines resulting in the trapping of the incident plasma they carry initially. Electrons at ~90° pitch angle may subsequently be pushed into the loss cone by wave-particle interactions, static, or time varying electric fields, resulting in the conics. BECs may also be generated by mirroring of the particles that are streamed to lower altitudes on nearby open field lines, which then diffuse and/or scatter onto inner closed field lines.

Citation: Ulusen, D., D. A. Brain, and D. L. Mitchell (2011), Observation of conical electron distributions over Martian crustal magnetic fields, *J. Geophys. Res.*, *116*, A07214, doi:10.1029/2010JA016217.

1. Introduction

[2] Mars is a weakly magnetized solar system body with a substantial ionosphere. Therefore on a global scale its interaction with the solar wind is an example of a typical unmagnetized body interaction (such as the Venus interaction) [*Luhmann*, 1986]. As the upstream solar wind plasma deviates around the body, the Interplanetary Magnetic Field (IMF) frozen into the plasma drapes around the conducting ionosphere forming a two-lobed induced magnetotail downstream [*Luhmann and Brace*, 1991; *Nagy et al.*, 2004]. Although the main obstacle to the solar wind is the Martian ionosphere, the strong crustal magnetic fields localized mainly in the southern hemisphere on Mars also interact with the solar wind [*Mitchell et al.*, 2001; *Acuña et al.*, 1998]. This interaction creates several local dynamic and transient events, many of which are the Martian counterparts of events observed on Earth, such as daytime and nighttime auroral events [*Bertaux et al.*, 2005], temporary trapped radiation [*Mitchell et al.*, 2001], local electron flux enhancements [*Soobiah et al.*, 2006; *Ulusen and Linscott*, 2008b], magnetic reconnection [*Krymskii et al.*, 2002], and conical electron distributions [*Brain et al.*, 2007]. This paper focuses on analysis of one of these phenomena, conical electron distributions, which were first reported near the strong crustal sources at Mars by *Brain et al.* [2007].

[3] On Earth, several different types of electron distributions referred to as conics have been observed since their discovery in Dynamics Explorer 1 (DE 1) data by *Menietti and Burch* [1985]. An electron conic is defined as an angular flux distribution having peaks oblique to the local magnetic field direction. Most of the observations in DE and Viking data reported previously are monodirectional conics having a peak outside the loss cone in the upward going electron flux at the highest energy present (these are referred to as just "conics" in the literature). A number of observations have bidirectional peaks in the electron flux at the same energy moving in both upward and downward directions [*Lundin et al.*, 1987; *Menietti et al.*, 1992, 1994; *Menietti and Weimer*, 1998; *Eliasson et al.*, 1996; *Burch et al.*, 1990; *Hultqvist et al.*, 1988]. Both types of conical distribution are observed on the dayside and nightside above the polar caps and auroral ovals (between 8000 and 11,000 km altitudes)

[1]Space Sciences Laboratory, University of California, Berkeley, California, USA.

0148-0227/11/2010JA016217

and they are both associated with trapped particles, potential drops, ions beams, or ion conics. Variety in the characteristics of the observed conical distributions demonstrates the complexity and variability of the auroral acceleration processes as well as the plasma processes responsible for ionospheric escape. Therefore a number of different mechanisms have been proposed for their generation including perpendicular or oblique heating due to wave-particle interactions (analogous to ion conics [*Menietti and Burch*, 1985; *Menietti et al.*, 1992; *Wong et al.*, 1988; *Roth et al.*, 1989]), parallel heating due to field aligned potential or wave-particle interactions [*Burch et al.*, 1990; *Burch*, 1995; *Roth et al.*, 1989; *Temerin and Cravens*, 1990; *André and Eliasson*, 1992; *Thompson and Lysak*, 1994], and acceleration due to time-varying field-aligned electric fields [*Lundin et al.*, 1987; *André and Eliasson*, 1992].

[4] At Mars, previous satellite observations over the crustal sources have shown auroral-like emissions and peaked electron energy distributions implying that regions of radial crustal field exhibit similar signatures to Earth's cusp regions [*Bertaux et al.*, 2005; *Leblanc et al.*, 2006; *Dubinin et al.*, 2008; *Brain et al.*, 2006a; *Lundin et al.*, 2006]. This suggests that the same acceleration mechanisms, plasma-wave interactions, and ionospheric escape processes may operate at Mars and therefore we might expect to observe similar associated electron flux distributions. In fact, bidirectional conical distributions having peaks both in the upward and downward moving electron fluxes have been reported in Mars Global Surveyor (MGS) data previously, as well as monodirectional conical distributions with peaks in the upward moving flux and incident distributions that are either isotropic or field-aligned beams [*Brain et al.*, 2007]. This paper presents results from the first study of the detailed characteristics of these observations and their generation mechanism. We focus on bidirectional conical distributions, determine their features and operating conditions, discuss the main similarities and differences between Mars and Earth observations, and provide a physical explanation for their occurrence. Revealing the actual formation mechanism behind the electron conical distributions is important for understating the sources and sinks of the ionosphere as well as the state and evolution of the upper atmosphere at Mars. In addition, association of these observations with the crustal fields shows the influence of the crustal sources on the Martian plasma interaction and a study of this influence allows us to understand the Martian nightside region better.

[5] In this paper, section 2 describes the data used in this study. Section 3 introduces the electron conic observations at Mars and compares them to Earth observations. Section 4 gives geographical distributions and section 5 analyzes one electron conic example in detail describing its detailed features. Section 6 gives statistical analysis of the observations in addition to their IMF dependence. Section 7 discusses possible formation mechanisms and includes our interpretation of the observations. And finally section 8 gives a brief summary and discusses future directions.

2. MGS Data

[6] This study is based on observations from the MGS Magnetometer/Electron Reflectometer (MAG/ER) instrument. The MGS MAG/ER instrument consisted of two redundant triaxial fluxgate magnetometers (MAG) and an electron reflectometer (ER) (for details, see *Acuña et al.* [1992] and *Mitchell et al.* [2001]). The MAG provided vector measurements of the in situ magnetic field at rates up to 32 samples per second over a dynamic range from (+/−)4 nT to (+/−)65,536 nT with a typical instrumental noise level of ~0.5 nT at night, and ~1 nT in sunlight. The ER measured the local electron distributions over a 360° × 14° disk-shaped field of view in 16 angular sectors (each 22.5° wide) and 19 different energy channels between 10 eV and 20 keV every 2 s, with an energy resolution of 25%. Detailed description of the MGS MAG/ER instrument and data processing can be found in the work of *Acuña et al.* [1992, 2001]. Electron flux distributions with respect to the local direction of the magnetic field, in other words pitch angle distributions (PADs), can be determined from coupled MAG and ER measurements every 2, 4, or 8 s. Since the orientation of the local magnetic field with respect to ER varies and the MGS spacecraft did not spin, only 2-D PADs with a variable width can be obtained [*Mitchell et al.*, 2001].

[7] In this study, more than 7 years worth of magnetometer and electron reflectometer (MAG/ER) data were used, acquired during the MGS mission's mapping phase between July 1999 and November 2006. During the mapping phase, the polar orbit of MGS was nearly circular at a nearly constant altitude of ~400 km, fixed at 0200–1400 local time, with MGS completing an orbit every 2 h and orbiting almost 12 times in one Martian day [*Albee et al.*, 2001].

3. Detection of Conical Electron Distributions

[8] Previously, more than 60 million pitch angle distributions obtained from the MGS mapping phase MAG/ER data were analyzed by *Brain et al.* [2007] in an attempt to construct a geographic map of the local magnetic topology. In their analysis, pitch angle distributions were categorized into 26 different types of PADs considering their shape, and electron conic like distributions at Mars were reported among these categories. In our study, we use the same method to detect the electron conics in MGS data and analyze these observations to study their characteristics and formation mechanisms.

[9] ER records PADs in 19 energy channels between 10 eV and 20 keV; however, electron conic signatures are observable typically at energies between ~90 eV and ~640 eV. From the ER data it is not possible to reliably determine whether the reason for undetectable conic signatures at low-energy and high-energy channels is instrumental or if it is the nature of the events. The signal-to-noise ratio of the PADs at high energies (>500 eV) is low due to low electron flux levels and the measurements at low energies can be contaminated by the spacecraft potential, attenuator, and secondary electrons generated at the spacecraft through photoionization or particle impact [*Brain et al.*, 2007]. Therefore in this study we primarily use data from the energy channel at 115 eV, which is representative of the energy channels at which the electron conic signatures are clearly observed.

[10] In obtaining a PAD for each MGS measurement, we map the field of view (FOV) of the ER into pitch angle using the magnetic field measurements. In-flight calibration (see discussion by *Mitchell et al.* [2001]) yielded flux measurements accurate to within ~5–10% for most sectors but 10–15% for two sectors significantly affected by FOV

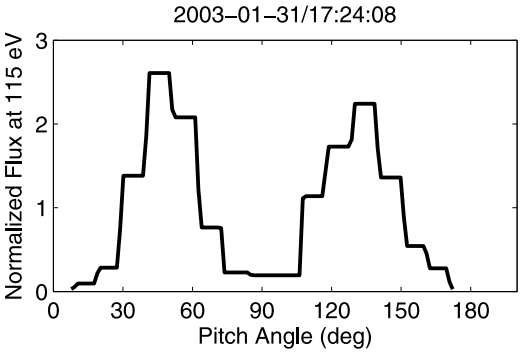

Figure 1. One typical PAD example of the electron conics observed by MGS from the 115 eV energy band on 31 January 2003.

blockage from the solar array gimbal and the spacecraft bus. Since the range of pitch angles measured by ER at any given moment is sampled twice (ER has a 360° FOV but pitch angles goes from 0° to 180°), we conservatively chose to omit data from these two sectors without substantial loss of information (and preventing possible identification of "features" in the PAD due to calibration issues). The pitch angle coverage is reduced only when the two masked sectors are at the minimum or maximum pitch angles. Next, background noise estimated from each measurement is subtracted from the ER data in all sectors. Then the data for each observation are resampled into 128 equal-sized pitch angle bins (using simultaneous MAG data) ranging from 0° to 180°. "Normalized flux" for each measurement is obtained by calculating an average flux from all 128 bins and dividing the flux at each bin with this average value. Observations with poor statistics resulting from a variety of uncertainties, such as instrument saturation, statistically insignificant count rates, the ambient field direction (corresponding to field magnitudes of less than 12 nT), or the width of the measured PAD (smaller than 90°) are excluded in the present analysis. In all, 43% of the available observations meet our selection criteria and are sorted as "usable observations." Detailed description of this selection process can be found in the work of *Brain et al.* [2007]. In order to separate BECs out of these usable observations, two halves of a PAD, from 0° to 90° and from 90° to 180°, are treated separately. Observations having flux levels at the intermediate pitch angles in the two halves exceed the flux at 90° pitch angle by more than 2.58σ are recorded as bidirectional electron conics.

[11] Over a period of 7 years, we detected ~150,000 bidirectional electron conics by using the above method in the MGS mapping data at ~400 km altitude. One typical example of an electron conic detected on 31 January 2003 is shown in Figure 1. The staircase nature of this plot is due to the fact that adjacent bins that are mapped to the same ER sector sample the same flux level. In addition, for this measurement, the local magnetic field is aligned slightly away from the center of one of the ER sectors resulting in uneven number of bins having the same flux level at both sides of the PAD. As seen in Figure 1, the electron flux at 115 eV is enhanced at oblique angles, having peaks at 65° and 115°. For a typical conic event in MGS data, these peaks are symmetric about 90° pitch angles and located between 35°–70° and 110°–145°. As evident in Figure 1, conical distributions analyzed in this study are bidirectional, with upgoing and downgoing electrons having about the same flux. This feature is representative for the energy range over which we observed these events, between ~90 eV and ~640 eV. Outside of this band for the lower-energy and higher-energy channels of ER we do not observe clear conical distribution signatures. The conical distributions at Earth having features similar to the observations we analyze in this paper were reported in Viking data by *Lundin et al.* [1987] and in DE 1 data by *Burch et al.* [1990]. Taking into account the classification scheme proposed for the many different types of conics in the work of *Lundin et al.* [1987], we call these events "bidirectional electron conics" (referred to as BECs hereafter). Common features of this type of conic include the energy band of the observations, the location of the peaks about the 90° pitch angle, and the relative magnitude of the peaks with respect to the flux at 90° pitch angle. Details of these features will be discussed in the following sections. First, the geographical distribution of these events and their association with the strong crustal sources are studied in section 4.

4. Geographical Distribution

[12] To examine the geographical extent and the occurrence likelihood of electron conics, we examine the percentage of BECs out of all observations as a function of location. Then we classify location as Martian darkness (solar zenith angle (SZA) > 120°, as SZA = 120° corresponds roughly to the eclipse boundary at 400 km altitudes), over the terminator (60° < SZA < 120°), and on the dayside (SZA < 60°) are obtained as a function of geographical location. Percentages are obtained by determining the ratio of the number of BECs to the total number of usable observations obtained by MGS. From these percentage maps we find that BECs detected from 115 eV electron flux measurements are observed mostly in darkness and over the terminator but less frequently on the dayside. The total number of electron conics observed over 7 years is ~150,000, 60% of which are observed in darkness (Figure 2), 25% are observed over the terminator, and ~15% are observed on the dayside. The maximum number of observations is ~105 observed at 10°S, 165°E with an occurrence rate of 35% in shadow. This feature implies that the physical conditions that favor the formation of conical PADs occur more frequently in darkness and/or MGS MAG/ER is not be capable of detecting all conics on the dayside. One likely reason for the lower conic detection rate on the dayside may be constant dayside photoionization, which can cover the BEC signatures by producing isotropic PADs with dominating photoelectrons. As the governing processes are more complex and the conic observation rate is relatively low over the terminator region, we focus on the observations in darkness for the rest of this paper.

[13] In eclipse, conics are clearly observable between 115 eV and 515 eV. Percentage maps for the occurrence of BECs at each energy channel, similar to the one shown for 115 eV in Figure 2, are obtained for all other energy levels of ER (not shown here). Analysis of these maps shows that the typical energy detection range of the BECs is from ~90 eV to ~640 eV. However, we noted previously that it is not possible from the ER data to determine whether the absence of

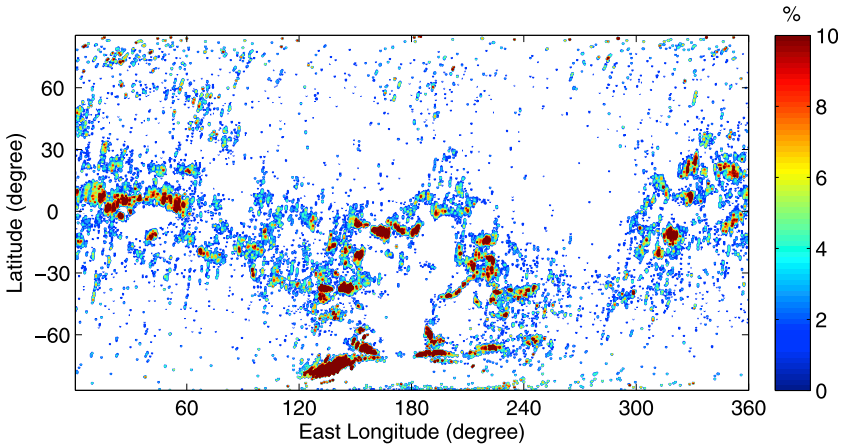

Figure 2. Map of the percentage of bidirectional electron conics out of all usable observations in Martian darkness (SZA > 120°).

the electron conics at low and high energies is a real effect or due to instrument limitations. In Figure 3, black dots mark the locations on a 0.5° × 0.5° bin geographical map where a bidirectional electron conic is observed at least once in the 7 years of MGS observation. This map was then superimposed on a map of the crustal magnetic fields, the strength of which are calculated from Cain's spherical harmonic model over a spherical surface at 400 km altitude and color coded in Figure 3 [*Cain et al.*, 2003]. One evident feature in Figure 3 is that nighttime BECs are associated with the crustal anomalies. They are mostly observed over moderately strong crustal magnetic fields, avoiding the regions having strong sources. In section 5 we will study the characteristics of BECs in detail by presenting a case study having the spacecraft trajectory plotted in Figure 3 (magenta line).

5. Case Study

[14] In this section, we analyze the data from an MGS nighttime pass on 19 July 1999 in order to study the characteristics of BECs in detail. We selected this particular case as in this region the BEC observation frequency is high (Figure 2) and typical BEC signatures are clearly observable. Figure 4 shows time series ER/MAG data as MGS passes over the portion of the trajectory indicated by the magenta line in Figure 3. During this portion of the MGS orbit, the ER instrument sampled three different types of PAD near the crustal sources. (The variation in the PAD width is due to the variation in the relative orientation of magnetic field and spacecraft.) First, BECs are clearly observable between 5°N and 1°S (centered at ~1104 UT/solid magenta line at T3) with peaks at around 40° and 130° pitch angles. Second, in the surrounding regions centered at 7°N and at 6°S (at around T2 and T4, respectively), the PADs have trapped characteristics (two-sided loss cone). Third, the electron angular distributions around T1 and T5 show isotropic distribution signatures over the range of pitch angles sampled by ER at that time. As seen in Figure 4a, electron fluxes are almost one order of magnitude higher at all energies in the regions of isotropic PAD, compared to the trapped and conic regions. Also note that before 1100 UT, MGS passes through a "void," where the electron flux drops to the

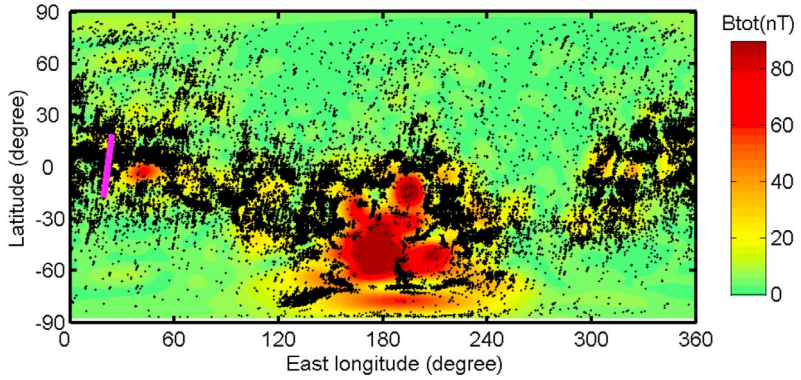

Figure 3. Spatial distribution of electron conics with respect to the crustal magnetic sources. Color map shows the magnitude of the crustal fields at 400 km altitude obtained from the Cain model [*Cain et al.*, 2003]. Black dots show the locations of 0.5° × 0.5° geographical bins where a bidirectional electron conic was observed at least once in 7 years. The magenta line indicates the portion of the spacecraft trajectory for the pass on 19 July 1999 during which an electron conic is detected by MGS ER which is analyzed in detail in section 5.

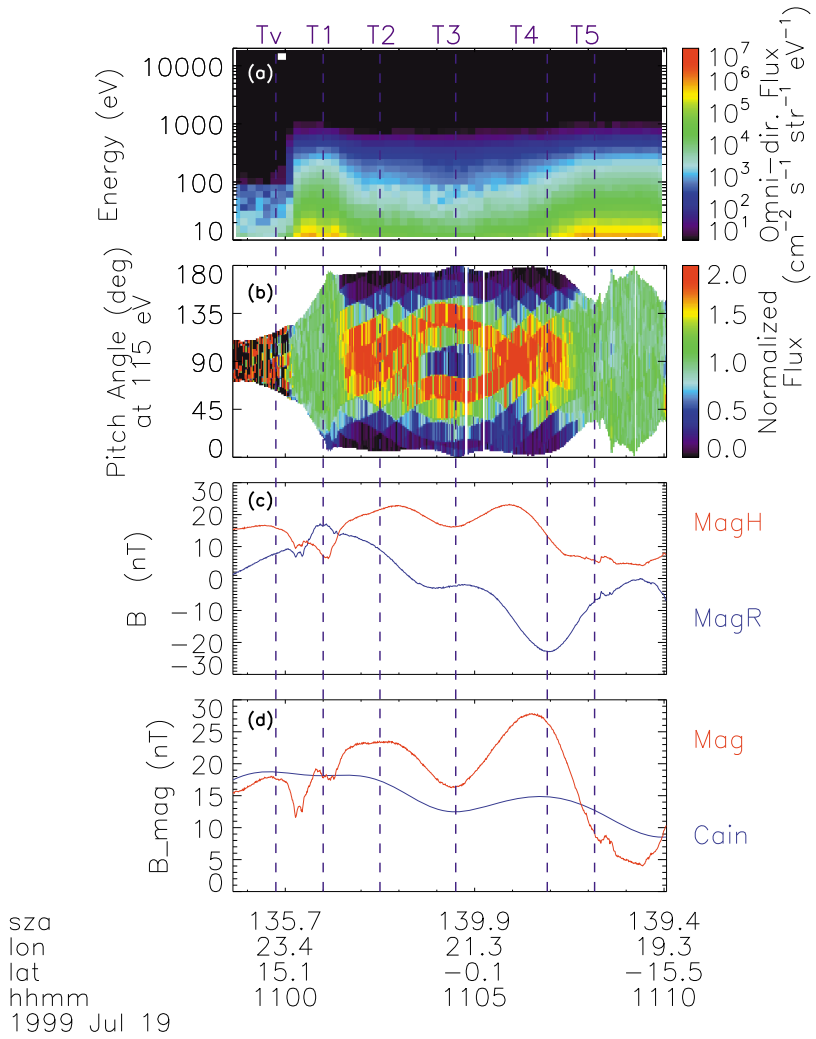

Figure 4. One example of nighttime electron conics observed on 19 July 1999. (a) Omnidirectional differential electron flux recorded by MGS ER. (b) Normalized pitch angle distributions recorded by ER at 115 eV. (c) Radial (MagR) and horizontal (MagH) components of the magnetic field recorded by MAG. (d) Magnetic field strength recorded by MAG and calculated from a spherical harmonic model by *Cain et al.* [2003].

instrumental background level in all energy channels as seen in Figure 4a [*Mitchell et al.*, 2001].

[15] The trapped distributions at T2 and T4 imply a closed field configuration. These regions surround the BECs at T3, which are observed on more horizontally oriented field lines than the surrounding regions. Therefore we infer that the BECs are likely to also occupy closed flux tubes. Over the areas surrounding the trapping regions (at T1 and T5) the magnetic field is mostly radial, with either isotropic PADs or one-sided loss cones. We infer that these field lines are likely to be open, with access to the tail or the magnetosheath [see *Brain et al.*, 2007]. Moreover, at around T1 and T5 there are perturbations in the measured field (local oscillations in the red curve) suggesting the presence of currents at the boundary between the open and closed field regions [*Brain et al.*, 2006a]. As seen in Figure 4c, these perturbations are observed mainly in the horizontal field component, consistent with radial (field-aligned) currents in this region caused by downgoing incident electrons. Indeed, we observe electron acceleration signatures over the same regions. The perturbations and acceleration signatures observed at ~T5 are readdressed in the following paragraphs, where the electron energy spectra and PADs obtained from all energy cannels are presented and discussed thoroughly.

[16] Figures 5a–5c compare the electron energy spectra obtained at T3, T4, and T5, having BEC, trapped, and open field line PAD signatures, respectively. In addition, in Figure 5c, we also show a typical electron energy spectrum (red dotted line) obtained by *Mitchell et al.* [2001] from MGS measurements in the Martian magnetosheath. This representative sheath spectrum is very similar in shape to the "open field line spectrum" we obtained at T5 except that the latter has lower flux levels at all energies. This similarity implies that the field lines at ~T5 have access to the sheath. In Figures 5a–5c, we also plot "the open field line energy spectrum" detected at T5 for comparison to the spectra obtained during trapped and BEC events at T3 and T4. Figures 5a and 5b show electron energy spectra obtained in

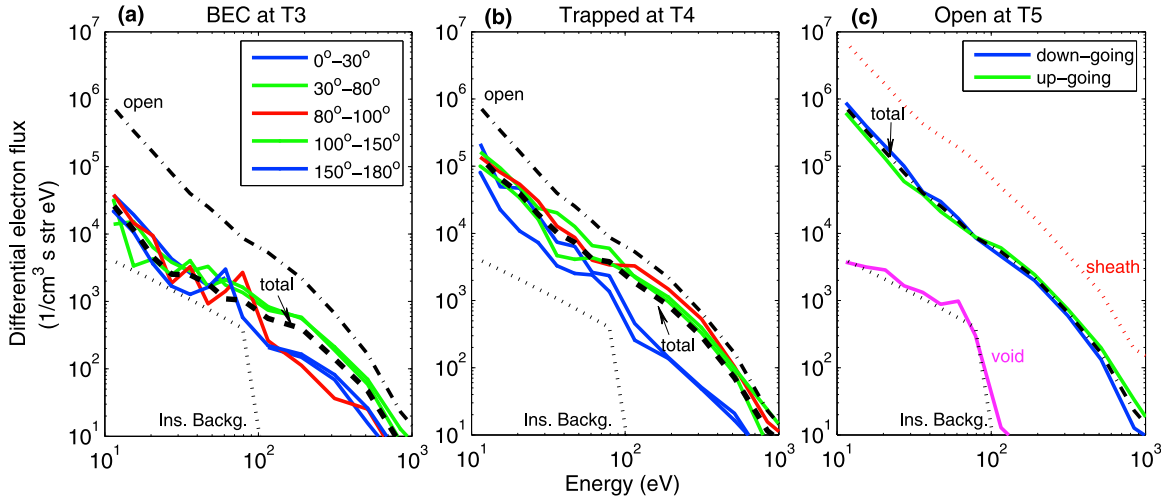

Figure 5. Comparison of the electron energy spectra obtained at (a) T3, (b) T4, and (c) T5 (indicated in Figure 4) having BEC, trapped, and open field line PAD signatures, respectively. The black dotted lines show the instrument background, and the dot-dashed lines show a typical spectrum on open field lines. In Figure 5c, the red dotted line shows a typical sheath spectrum obtained by *Mitchell et al.* [2001], and the magenta line shows an example of a void spectrum recorded at Tv in Figure 4. Thick dashed black lines in Figures 5a and 5b indicate the total spectrum detected at T3 and T4. Colored solid lines show the spectra detected at T3, T4, and T5 in different pitch angle intervals as indicated in the legends.

different pitch angle intervals: (1) in the loss cone [0°–30° and 150°–180°]; (2) along the pitch angles where the BEC peak [30°–80° and 100°–150°]; and (3) at around 90° pitch angle [80°–100°]. The most obvious feature in Figures 5a and 5b is the substantial decrease in the conic and trapped flux at all energies compared to neighboring open field lines (notice that the omnidirectional energy spectra shown by the black dashed lines for the conic and trapped PADs lie between the representative open and void spectra). Low-energy particles are significantly depleted for the BEC (the sharp variations in the low energy flux below ~100 eV are due to statistical fluctuations). This significant decrease in the electron flux (between 1 and 2 orders of magnitude) is typical for the trapped and conical distributions observed in darkness. We expect closed field regions to have reduced electron flux because they are isolated from a continuous source of suprathermal electrons compared to open field regions, which have access to electrons in the magnetotail or sheath. Electrons in the closed field regions must have originated either in the surrounding regions (and been transferred to closed field lines) or have already been trapped on these field lines at earlier times. We will discuss this feature in section 7 in more detail. The symmetric nature of the PADs from BEC and trapped regions is evident from the directional fluxes in energies above 100 eV (blue and green curves in Figures 5a and 5b). For both regions the spectra are similar except at around 90° pitch angle. The BEC flux perpendicular to the field line is depleted substantially (red curve in Figure 5a). These features are common for almost all electron conic observations in darkness.

[17] As mentioned in section 3 and as can be seen clearly in Figure 4b, BEC signatures are easily detectable at 115 eV. To reveal the energy range over which the electron conic signatures are visible, in Figure 6 we show the angular distribution of the unnormalized flux at 19 energy channels recorded for the BEC event from Figure 4. The electron angular distributions at different energy channels at around T5 reveal an interesting feature of the regions we have identified as open. At low energies (10 eV and 47 eV, last five panels of Figure 6), the downgoing electron flux is higher than the upgoing flux implying that incident electrons at this energy are not reflected back effectively although their pitch angles lie outside the loss cone (at higher energies the upgoing flux at the same pitch angles is evident). At intermediate energies (61 and 190 eV), the PADs are isotropic. At higher energies, (313 and 515 eV), the upgoing electron flux is higher than the downgoing electron flux. This feature can also be seen in Figure 5c where the total downgoing (blue line) and total upgoing (green line) electron fluxes are plotted together. As seen the downward flux is higher for low energies and the trend reverses for higher energies. In addition, as evident in Figure 6, the low-energy downgoing electrons (between 11 eV and 47 eV) populate a narrower pitch angle range between 0° and 90° while the high-energy up-coming electrons (between 191 eV and 515 eV) have pitch angles distributed more evenly between 90° and 180°. This behavior implies that low-energy incident electrons may be accelerated by perpendicular or oblique heating (an increase in the electron velocity in a direction perpendicular or oblique to the local magnetic field) and reflected back at higher energies. Simultaneous ion measurements could help us to determine the existence of an electric field responsible for such heating, as well as its direction and strength in the vicinity of the acceleration region. Unfortunately, MGS did not measure ions. Furthermore these incident accelerated electrons may be the source of the trapped and BECs particles on neighboring closed field

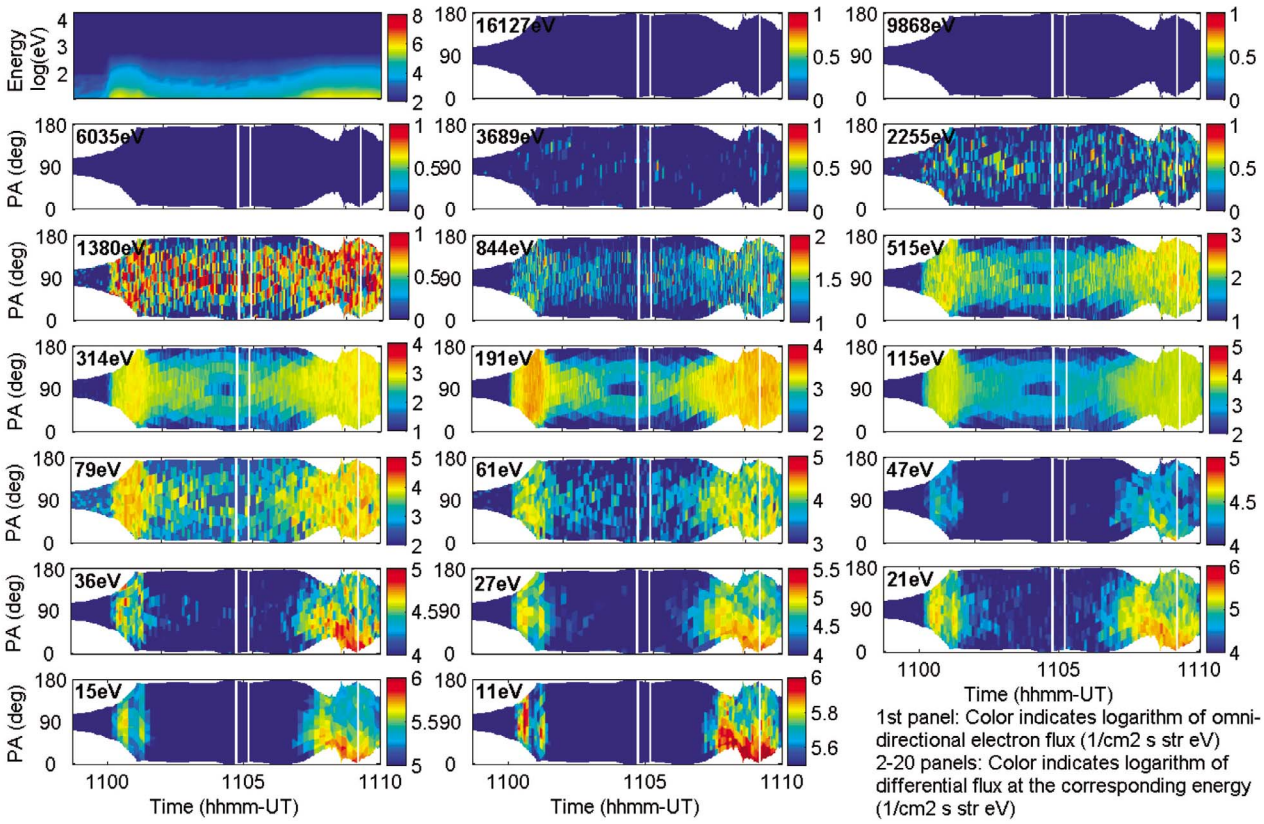

Figure 6. One example of the nighttime electron conics observed on 19 July 1999 and shown in Figure 4. The first panel shows the omnidirectional differential electron flux recorded by MGS ER. The following 19 panels show the directional differential electron flux (on a logarithmic scale) as a function of pitch angle and time for different ER energy channels.

lines. Possible mechanisms responsible for the generation of BECs will be discussed in section 7.

6. Statistical Analysis

[18] In this section we statistically analyze the ~90,000 BEC observations in shadow in order to explore their dependence on the ambient magnetic field structure as well as upstream conditions (draping direction of IMF, solar wind pressure, and EUV flux).

[19] Figure 7a shows the distribution of electron conics as a function of ambient magnetic field strength, and Figure 7b shows the same distribution as a function of elevation angle of the ambient magnetic field. The field strength is about 15 nT and elevation angle is mostly small (<45°) during conic events, implying they are more likely to occur above the moderate horizontal crustal fields. The preference for horizontal field lines along with the symmetric PAD with loss cone signatures imply that BECs form on closed field lines.

[20] In this section we also explore the dependence of the electron conics on the varying upstream conditions, including IMF direction, solar wind pressure, and EUV flux. As there is no instrument on board MGS to measure the upstream parameters, in our analysis we use proxies for IMF draping direction and solar wind pressure described by *Brain et al.* [2006b] and a proxy for EUV flux obtained by *Mitchell et al.* [2001].

[21] In 2005, *Brain et al.* [2006b] first proposed a method of estimating the IMF draping direction from MGS data.

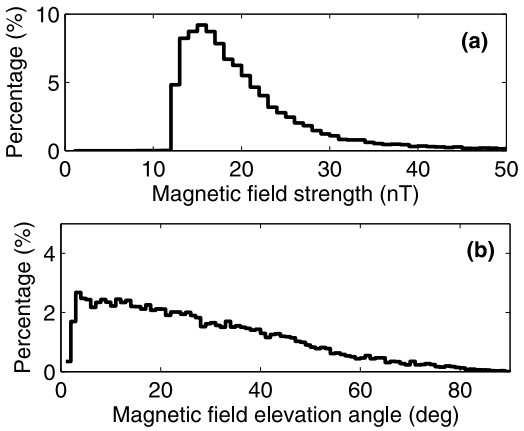

Figure 7. (a) Percentage of occurrence of nighttime electron conics as a function of magnetic field magnitude (in nT) and (b) percentage of occurrence of the nighttime electron conics as a function of local magnetic field elevation angle (in degrees).

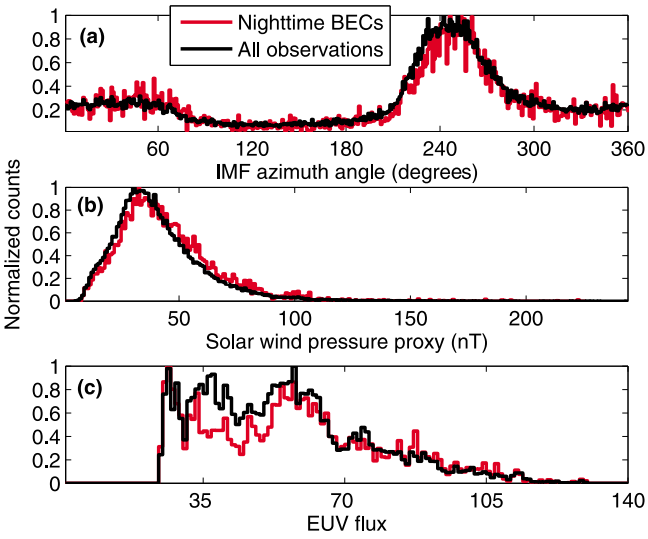

Figure 8. Dependence of nighttime electron conics on the upstream conditions. Red curves represent the distributions at the time of conics, and black curves represent all observations in 7 years. (a) Dependence on the draped IMF azimuth angle. (b) Dependence on the solar wind pressure. (c) Dependence on the EUV flux.

The angle (azimuth angle) between the horizontal component of the local magnetic field (with respect to the surface) and the MGS orbit direction was calculated using the magnetic field measurements recorded on the dayside over the Northern Hemisphere (where crustal fields are negligible in the latitude band between 50° and 60°N). Although the IMF direction changes on many timescales and an estimate obtained from a small portion of the orbit does not necessarily represent the orientation throughout the entire orbit, for our purpose we assume that the IMF was constant over an orbit and the calculated azimuth angle represents the draping direction. In Figure 8a, red lines show the histogram of the IMF azimuth angle (normalized by the maximum number) at the time of the conics while the black lines show the normalized histogram of the same angle obtained from all orbits in 7 years, determined using the method described above. As evident in this plot, distribution of the IMF direction during the conics is not different from the general distribution of the IMF, implying that the conics do not depend on the IMF draping direction.

[22] Similarly, to obtain an estimate for the solar wind pressure, *Brain et al.* [2005] calculated subsolar field strength for every orbit of MGS during the 7 years of mapping observations. In this calculation MGS data recorded over the crustal sources and data having SZAs > 110° were excluded. The remaining data were fit to a cos(SZA) function to extrapolate to the field magnitude at SZA = 0°. (These results agree well with the pressures estimated using the magnetic field from the pileup region by *Crider et al.* [2003].) In this work the proxies are specified in the units of field strength rather than in pressure, which should be sufficient for distinguishing times of low and high upstream pressure, assuming that pressure does not change too much over an orbit. Utilizing these calculated proxies, in Figure 8b we obtain the histogram of the solar wind pressure at the time of the conics (red line) and compare it to the solar wind pressure distribution (black line) obtained from all orbits over the entire MGS mapping period. In Figure 8, although the distribution of BECs is slightly lower than the distributions for all orbits between 30 and 80 nT, a chi-square test of the distribution shows that the BEC occurrence rate is at most weakly dependent on the solar wind pressure variations.

[23] Possible correlation between the observation of BECs and EUV flux level at Mars would imply that the source of the electrons of the observed conical distributions may be the sunlit regions of Mars. We compare the EUV flux distribution for the electron conics (red line) with the EUV at Mars over the entire mapping period (black line) in Figure 8c. We use a proxy for EUV flux determined by scaling F10.7 flux measurements at Earth by $1/r^2$ to account for the Mars' orbital distance from the Sun and then time shifting these values to account for the solar longitude difference between the Earth and Sun [*Mitchell et al.*, 2001]. As evident in Figure 8c, BEC occurrence is slightly depleted during periods of moderate EUV flux, but a chi-square test shows that this dependence is weak. We have no plausible explanation for this depletion in the BEC distribution.

[24] From the comparisons in Figure 8, we conclude that in general BEC occurrence is at most weakly dependent on variations in the upstream conditions. Observation of BECs over the same geographical locations for many sequential passes that are separated by days with a variety of upstream parameters implies the stability of the events (refer to Figure 2). This stability also suggests that the driving processes of BECs more likely to operate on the crustal field lines.

7. Physical Interpretation of the Observations

[25] In this section, possible physical explanations for the electron conic observations are discussed. In previous sections, we show that the BECs are more likely to occur on closed field lines and are mostly surrounded by trapping regions, whose signatures are clearly visible in the same energy range as the BECs (Figures 5 and 6). In Figure 9a, we compare the angular distribution of 115 eV electron flux obtained at T2, T3, and T4 for the case presented in Figure 4, which clearly shows the depletion of electrons at around 90° pitch angle for the BEC. The resemblance of the BEC and trapping distributions at angles within ~40° of being field aligned implies the possible relationship in the source mechanism of these events.

[26] Although there are differences between the Cain model predictions and MGS magnetic field measurements (as the Cain model describes crustal sources and excludes external effects), analysis of the field line distribution obtained from the model still gives insight about the field configuration near the observations. In Figure 9b, the field lines obtained from the model near the BEC given in Figure 4 are shown in blue. We obtained these field lines by starting to trace them at points on the MGS trajectory that are separated by ~1°. The MGS trajectory (black dashed line) and the portion of the trajectory (marked in red) for which the data is provided in Figure 4 are shown in Figure 9b. The location of the BECs in Figure 4 corresponds to the innermost closed field lines in the region, consistent with our interpretation in the previous paragraphs. Using the modeled

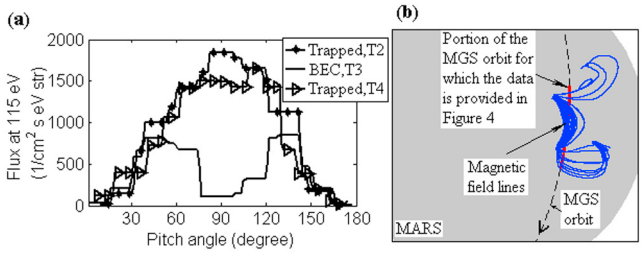

Figure 9. (a) PADs obtained by MGS ER at times T2, T3, and T4 in Figure 4. (b) Magnetic field lines (blue) obtained from the Cain model [*Cain et al.*, 2003] near the BEC observation site given in Figure 4. Dashed line indicates the trajectory of MGS, and red portion of the trajectory corresponds to the time period for which the data is provided in Figure 4.

field lines, we analyze the variation of the electron PADs as they evolve adiabatically along the field line. This analysis allows us to roughly determine the altitude range over which BECs can be observed.

[27] In order to estimate this altitude range, we select the field line that MGS occupies at T3 Then we apply the first adiabatic invariant (equation 1, where B_1 and B_2 represent the field strength at two arbitrary altitudes of h_1 and h_2 on a closed field line and α_2 is the corresponding pitch angle at h_2 for the particles having pitch angles of α_1 at h_1) to determine how the PAD shape varies along

$$\frac{\sin^2(\alpha_1)}{B_1(h_1)} = \frac{\sin^2(\alpha_2)}{B_2(h_2)} \qquad (1)$$

this field line below the 400 km altitude of observation. (Conservation of the first adiabatic invariant (equation (1)) let us calculate the PAD distribution of electrons on a field line at altitudes below the point at which the PAD is known. This means that if the PAD is known at the minimum B point on a closed field line, the PAD can be determined everywhere on this field line.) Our analysis shows that on the field line we selected, the PAD first changes from a BEC with peaks separated by ~90° to a BEC with closer peaks having decreased flux levels. Then it turns into a two-sided loss cone as one moves to lower altitudes along the same field line. By this analysis we find that the altitude at which the shape of the PAD changes from a BEC to a two-sided loss cone is ~280 km. As the peaks of the observed BECs are located at similar angles (between 35°–70° and 110°–145°) and the strength of the minimum B fields on which BECs are observed is similar (~15 nT at 400 km altitude), we expect that the PAD transition altitude is close to ~280 km for all observations. In other words BECs can be observed at altitudes down to ~280 km.

[28] The close relationship of trapped and BEC distributions is further examined by the analysis of PADs obtained at sequential passes of MGS over a conic observation site with high BEC occurrence probability. This analysis shows that a BEC almost always forms with similar signatures over the same location. For passes not showing BECs we mostly observe high fluctuations in the magnetic field and an increase in the electron flux, possibly indicating nonstandard conditions such as solar storms during these passes. Over the geographical locations having lower BEC occurrence rates, trapped distributions are observed as frequently as BEC distributions. Furthermore, we occasionally observe voids at the center of the trapped distributions. In order to show the association of trapping regions with the BEC observation sites, we obtain a geographical map in Figure 10 where the black dots mark the locations of nighttime trapped electrons observed at least once in 7 years. Similarly, the orange dots which are plotted on top of this map indicate the regions where we observe a BEC at least once in 7 years. This map shows that trapping sometimes occurs in almost all locations where a BEC has been observed. However, in the regions of high BEC occurrence probability (see Figure 2), trapping is less likely to occur. Another interesting feature evident on this map is that there are quite a number of locations where we observe trapped distributions but not BECs.

[29] Considering the PAD distributions observed in the vicinity of the BECs, we propose a field configuration near a BEC region as illustrated by a cartoon in Figure 11a. This configuration is consistent with the field lines obtained from the Cain model in Figure 9b. In the proposed field config-

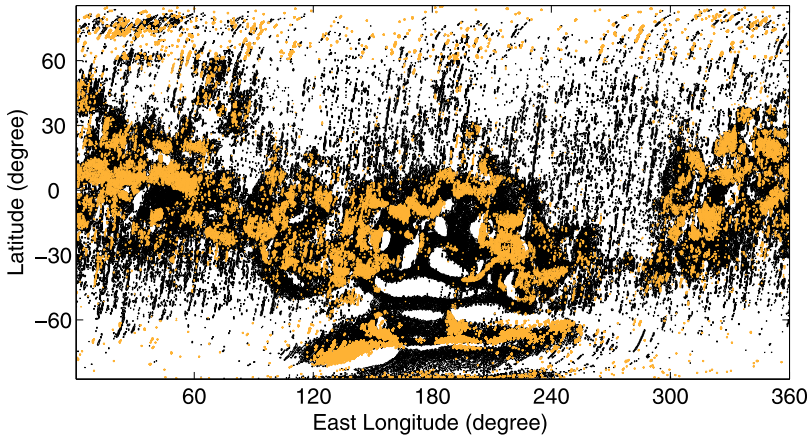

Figure 10. Association of BECs observation locations with the trapping regions. The black dots mark the locations of nighttime trapped electrons observed at least once in 7 years. The orange dots which are overplotted on the black dots indicate the locations of the BECs observed at least once in 7 years.

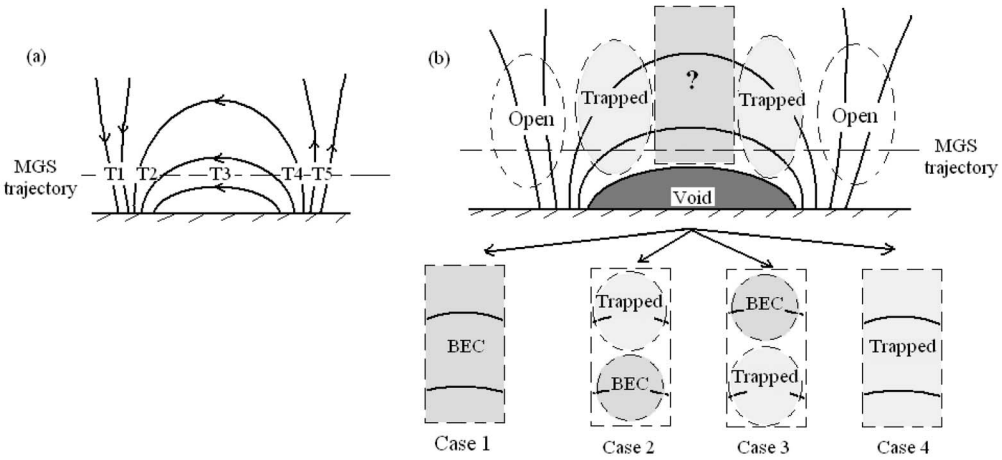

Figure 11. (a) Proposed magnetic field configuration near a BEC observation site. (b) Regions of different PADs in the field configuration shown in Figure 11a. There are four possibilities for the generation of different PADs in the middle section of the closed field lines.

uration in Figure 11a there is a closed field region in the center and it is surrounded by open field lines. The position of the MGS orbit is shown by the dashed line, and on this line, we also mark the locations of MGS at times T1, T2, T3, T4, and T5. Considering our interpretations in the previous sections, in this configuration plasma is incident on the outer open field lines and the closed field lines that are strongest and closest to the surface form "voids." Above the voids, the side portions of the closed field lines that are near the "open" regions have trapped distributions. The constant altitude of MGS at 400 km prevents sampling the same observation site at different altitudes (unfortunately we do not have aerobraking data from these regions for SZA > 120°), preventing determination of the actual PAD distribution at all altitudes in the middle section of Figure 11b. This ambiguity yields the four possibilities for the electron angular distribution in Figure 11b. The middle section of the closed field lines has either BEC (case 1) or trapped (case 4) or a combination of a BEC and trapped distributions (case 2 and case 3). Here also note that there is in fact another possibility which is not included among the possibilities in Figure 11b; ER may record a "void" PAD in the middle section of the closed field lines when MGS passes through the interior closed field lines. The reason for ignorance of this scenario is that when it happens the regions above the voids can have exactly the same combinations of trapped or BEC distributions in cases 1, 2, 3, and 4. The observation of conical and trapped distributions on the closed field lines in Figure 11a may immediately suggest that the source of the particles is electrons generated on the dayside and trapped on these closed field lines as they rotate into darkness. If these electrons remain trapped when they move into shadow, they may contribute to generation of the BEC and trapped distributions. However, as estimated by *Ulusen and Linscott* [2008a], time scales of trapping and drift of electrons over the strongest field lines are much shorter (a few tens of minutes) than the rotation period of Mars. In their work, assuming that the atmospheric absorption altitude at Mars is ~150 km, *Ulusen and Linscott* [2008a] estimated the gradient drift velocity of 10 eV electrons over the strongest crustal sources (between 150°–215°E and 65°–30°S) as ~2 km/s and showed that these electrons can remain trapped inside these closed field lines for about 17 min. As MGS orbit is at 0200 LT sampling the regions that have been in darkness for several hours (~6 h), ~17 min trapping time suggests that the observed trapped and conical electrons are generated in Martian darkness shortly before their observation. Considering this, we propose three mechanisms for the formation of the BECs in darkness, which are illustrated in Figure 12.

[30] In the first scenario indicated by 1 in Figure 12, the outer field lines that are open and have access to the tail or magnetosheath merge. As a result the incident plasma on the low altitude portions of both field lines becomes trapped, forming a two-sided loss cone [*Brain et al.*, 2007]. During this process some fraction of the particles may be lost via a secondary process, either carried away with the merged field lines that have no connection with the surface or pushed into the loss cone as a result of possible heating during the merging process, resulting in a decrease in flux as MGS observed. When the conditions favoring the secondary process operate, BECs can be observed as in cases 1, 2, and 3 from Figure 11b. When they do not operate, case 4 is observed (only trapped distributions are formed). In the above scenario, depletion of the 90° electrons close to the minimum B point of a closed

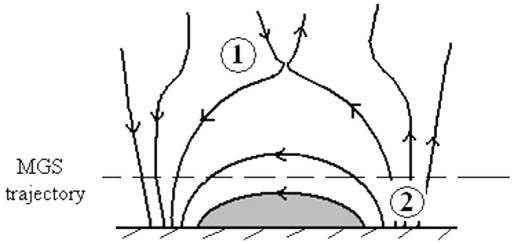

Figure 12. Possible formation mechanisms for the BECs in Martian darkness. Mechanisms 1 and 2 are discussed in the text.

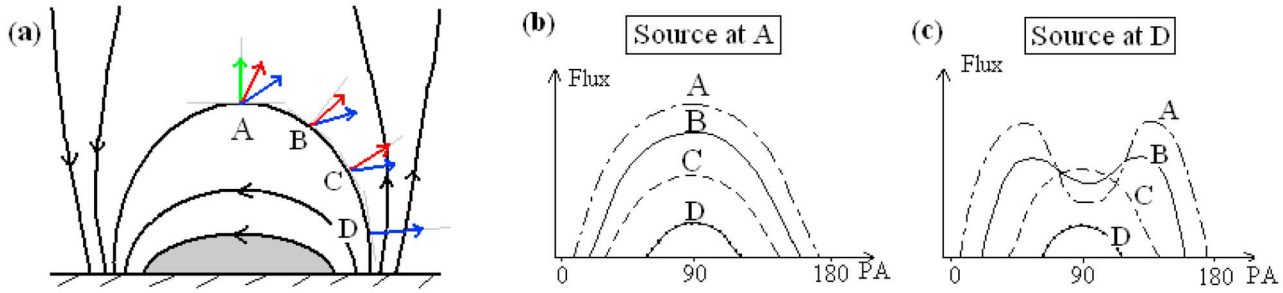

Figure 13. Explanation of the second formation mechanism proposed in Figure 12. (a) Proposed field configuration near a BEC observation site. (b) PADs that are expected to be observed at points A, B, C, and D shown in Figure 13a, when the electron source is at around A. (c) PADs that are expected to be observed at points A, B, C, and D when the electron source is at around D.

field line may involve wave-particle interactions and static or time-varying potential drops. Possible parallel heating (increase in the parallel velocity) due to such processes acting near the minimum B point of a closed field line may scatter the electrons from ~90° pitch angle toward 0° and 180° pitch angles, forming the peaks of the BEC. This mechanism may also push some oblique electrons into the loss cone, where they are then lost in the atmosphere. Similar mechanisms have been suggested for the generation of the conics at Earth by *Burch et al.* [1990] and *Lundin et al.* [1987]. Using numerical simulations, Burch et al. showed that distributions similar to observed two-sided conics can form when the spacecraft passes through a region of field aligned electric fields. Verification of these source mechanisms would be possible by simultaneous electric field and/or ion measurements in the source region. (The gyrofrequency of the electrons near the horizontal field lines with strength of 15 nT is ~2.5 kHz.) Unfortunately, neither MGS nor Mars Express has the appropriate combination of instrumentation.

[31] In the second scenario indicated by 2 in Figure 12, some fraction of the particles that are incident on the open field lines may either diffuse to the neighboring closed field lines and/or they may scatter near the lower ionosphere and become trapped on the neighboring closed field lines. These two processes can directly create a PAD with depleted electrons at around 90° pitch angle. In a typical mirror configuration (Figure 13a), the location where the particles are injected into the mirror field and their initial PAD determine the final PAD of the trapped particles at any point on the field line assuming only adiabatic processes operate. In a typical case, when the particles are injected isotropically close to the minimum B point (A in Figure 13a), all PADs observed at every point along the field line will be a typical two-sided loss cone. PADs obtained at points A, B, C, and D for this typical case when the isotropic "source is at A" are shown in Figure 13b. However, when the source of electrons is at the foot of the closed field line as proposed in Figure 12 ("source at D" in Figure 13a), simple first adiabatic invariance implies a conic distribution near A, as detected by MGS ER. The reason for a conic distribution at A can easily be understood by noting the fact that on a closed field line electrons with pitch angles close to 90° at A cannot go far from A before mirroring. This means that when electron injection occurs only at the lower ionosphere (at D), electrons originating from this source region can only have low pitch angles at A resulting in a conical PAD (curve indicated by A in Figure 13c). Moreover, a conical distribution at A will still result in a BEC with closer peaks having lower flux levels at point B and a two-sided loss cone at point C and D The reason for this is that only the electrons with low pitch angles at A will reach B, C, and D with increased pitch angles (Figure 13c). Therefore BECs can be the result of the magnetic mirroring of the part of the incident electrons scattered/diffused in the lower ionosphere and become trapped on the neighboring closed field lines. This scenario explains case 1 in Figure 11b but not cases 2, 3, and 4.

[32] From MGS data it is not possible to determine unambiguously the actual source of the BECs out of the possibilities we listed above. In addition, electron conic signatures observed at each pass may have a different source mechanism unique to the location of the observation or all mechanisms listed here may operate simultaneously. Simultaneous observations of wave-particle data in the source regions and/or measurements at variable altitudes over the conic observation regions are needed for better understanding of the generation mechanism.

8. Summary and Future Directions

[33] The focus of this study is bidirectional conical distributions of electron flux detected in the MGS ER data at 400 km altitude observed at 0200 LT with SZA > 120°. The observed PADs at 115 eV are almost always symmetric about 90° pitch angle with two peaks between 35°–70° and 110°–145°. The signatures of BECs are clearly observable between ~90 eV and ~640 eV, yet it is still not clearly understood whether these events naturally do not occur at other energies or the instrument is not capable of detecting them. In this study, statistical results are obtained from 115 eV electron measurements, as this energy channel is representative of the entire observation band of BECs. Temporal and geographical distributions of the observations show that these conical distributions favorably occur in darkness in moderate horizontal crustal fields with strength of ~15 nT. These features and the two-sided nature of the PADs suggest that BECs form on closed crustal field lines. Furthermore, detailed analysis of separate events reveals that conics are surrounded

by trapping regions and their electron flux decreases substantially at all energy levels in relation to the neighboring regions that do not have conics but have access to either the tail or the magnetosheath.

[34] Exploration of the dependency of BECs on the upstream conditions shows that they do not depend strongly on the variations in the draped IMF direction, solar wind pressure, and EUV flux level. Observation of similar BECs over the same geographical locations for many sequential passes that are separated by days and have a variety of upstream parameters reveals the stability of the events. The independence of the BECs from the varying external conditions suggests that the driving processes of BECs more likely to operate in areas of crustal fields.

[35] We propose two main source mechanisms that may be responsible for the generation of BECs. In the formulation of these two proposals we have considered the fact that time scales of trapping and drift of electrons estimated over the strongest field lines are much shorter than the planet's rotation period. Therefore the observed trapped and conical electrons must be generated in Martian darkness shortly before their observation [*Ulusen and Linscott*, 2008a]. The first proposed mechanism involves the merging of open field lines neighboring the closed field lines on which trapping and BECs are observed. By this mechanism the incident electrons on the open field lines become trapped. Electrons at ~90° pitch angles can be either directly lost during the merging process or pushed to the loss cone by wave-particle interactions, static, or time varying electric fields. Similar mechanisms were proposed for the generation of the bidirectional electron conics observed at Earth [*Burch et al.*, 1990; *Lundin et al.*, 1987]. A second proposed mechanism involves the mirroring of particles that are streamed to lower altitudes on the nearby open field lines, which are then diffused and/or scattered into regions dominated by the inner closed field lines. Both mechanisms are consistent with the independent nature of BECs from the external conditions, yet verification of the role of these processes in the generation of the BECS requires simultaneous observations of waves, measurements of ions, and sampling of PADs at a variety of altitudes near the source regions.

[36] Analysis of dayside and terminator observations of MGS along with the ion data of Mars Express (ion composition, energy, and angular distributions) would help evaluate the potential drops at the measurement altitude. Such an analysis should be addressed in a follow up study. Other useful observations that would allow a more definitive statement to be made about the production mechanism of the conics are measurements of high-frequency variations in the magnetic and electric field. These measurements would help understand the wave activity and presence of particle acceleration nearby BECs. Future Mars Atmosphere and Volatile Evolution (MAVEN) spacecraft observations will provide more complete measurements of the definite characteristics of BECs, requiring further observational and theoretical studies to reveal the underlying mechanism of electron conics at Mars. Understanding generation mechanisms of the conics and plasma processes causing or resulting from them near the Martian minimagnetospheres will give better insight for different types of conical distribution observed at Earth or other planets with global magnetospheres.

[37] **Acknowledgments.** Thanks to Robert J. Lillis for preliminary simulation work in support of this research and thanks to Jasper S. Halekas for useful discussions. This study was supported by NASA grant NNX08BA59G.

[38] Masaki Fujimoto thanks Ying Juan Ma and another reviewer for their assistance in evaluating this paper.

References

Acuña, M. H., et al. (1992), Mars Observer magnetic fields investigation, *J. Geophys. Res.*, *97*(E5), 7799–7814, doi:10.1029/92JE00344.

Acuña, M. H., et al. (1998), Magnetic field and plasma observations at Mars: Initial results of Mars Global Surveyor mission, *Science*, *279*, 1676–1680, doi:10.1126/science.279.5357.1676.

Acuña, M. H., et al. (2001), Magnetic field of Mars: Summary of results from the aerobraking and mapping orbits, *J. Geophys. Res.*, *106*(E10), 23,403–23,417, doi:10.1029/2000JE001404.

Albee, A. L., R. E. Arvidson, F. Palluconi, and T. Thorpe (2001), Overview of the Mars Global Surveyor mission, *J. Geophys. Res.*, *106*(E10), 23,291–23,316, doi:10.1029/2000JE001306.

André, M., and L. Eliasson (1992), Electron acceleration by low-frequency electric field fluctuations: Electron conics, *Geophys. Res. Lett.*, *19*, 1073–1076, doi:10.1029/92GL01022.

Bertaux, J. L., F. Leblanc, O. Witasse, E. Quemerais, J. Lilensten, A. S. Stern, B. Sandel, and O. Korablev (2005), Discovery of aurora on Mars, *Nature*, *435*, 790–794, doi:10.1038/nature03603.

Brain, D. A., J. S. Halekas, R. Lillis, D. L. Mitchell, and R. P. Lin (2005), Variability of the altitude of the Martian sheath, *Geophys. Res. Lett.*, *32*, L18203, doi:10.1029/2005GL023126.

Brain, D. A., J. S. Halekas, L. M. Peticolas, R. P. Lin, J. G. Luhmann, D. L. Mitchell, G. T. Delory, S. W. Bougher, M. H. Acuña, and H. Reme (2006a), On the origin of aurorae on Mars, *Geophys. Res. Lett.*, *33*, L01201, doi:10.1029/2005GL024782.

Brain, D. A., D. L. Mitchell, and J. S. Halekas (2006b), The magnetic field draping direction at Mars from April 1999 through August 2004, *Icarus*, *182*, 464–473, doi:10.1016/j.icarus.2005.09.023.

Brain, D. A., R. J. Lillis, D. L. Mitchell, J. S. Halekas, and R. P. Lin (2007), Electron pitch angle distributions as indicators of magnetic field topology near Mars, *J. Geophys. Res.*, *112*, A09201, doi:10.1029/2007JA012435.

Burch, J. L. (1995), Dynamics Explorer observations of the production of electron conics, *Geophys. Res. Lett.*, *22*, 2705–2708, doi:10.1029/95GL02817.

Burch, J. L., C. Gurgiolo, and J. D. Menietti (1990), The electron signature of parallel electric fields, *Geophys. Res. Lett.*, *17*, 2329–2332, doi:10.1029/GL017i013p02329.

Cain, J. C., B. B. Ferguson, and D. Mozzoni (2003), An n = 90 internal potential function of the Martian crustal magnetic field, *J. Geophys. Res.*, *108*(E2), 5008, doi:10.1029/2000JE001487.

Crider, D. H., D. Vignes, A. M. Krymskii, T. K. Breus, N. F. Ness, D. L. Mitchell, J. A. Slavin, and M. H. Acuña (2003), A proxy for determining solar wind dynamic pressure at Mars using Mars Global Surveyor data, *J. Geophys. Res.*, *108*(A12), 1461, doi:10.1029/2003JA009875.

Dubinin, E. M., M. Fraenz, J. Woch, E. Roussos, J. D. Winningham, R. A. Frahm, A. Coates, F. Leblanc, R. Lundin, and S. Barabash (2008), Access of solar wind electrons into the Martian magnetosphere, *Ann. Geophys.*, *26*(11), 3511–3524, doi:10.5194/angeo-26-3511-2008.

Eliasson, L., M. Andre, R. Lundin, R. Pottelette, G. Marklund, and G. Holmgren (1996), Observations of electron conics by the Viking satellite, *J. Geophys. Res.*, *101*(A6), 13,225–13,238, doi:10.1029/95JA02386.

Hultqvist, B., R. Lundin, K. Stasiewicz, L. Block, P.-A. Lindqvist, G. Gustafsson, H. Koskinen, A. Bahnsen, T. A. Potemra, and L. J. Zanetti (1988), Simultaneous observation of upward moving field aligned energetic electrons and ions on auroral zone field lines, *J. Geophys. Res.*, *93*(A9), 9765–9776, doi:10.1029/JA093iA09p09765.

Krymskii, A. M., T. K. Breus, N. F. Ness, M. H. Acuña, J. E. P. Connerney, D. H. Crider, D. L. Mitchell, and S. J. Bauer (2002), Structure of the magnetic field fluxes connected with crustal magnetization and topside ionosphere at Mars, *J. Geophys. Res.*, *107*(A9), 1245, doi:10.1029/2001JA000239.

Leblanc, F., O. Witasse, J. Winningham, D. Brain, J. Lilensten, P.-L. Blelly, R. A. Frahm, J. S. Halekas, and J. L. Bertaux (2006), Origins of the Martian aurora observed by Spectroscopy for Investigation of Characteristics of the Atmosphere of Mars (SPICAM) on board Mars Express, *J. Geophys. Res.*, *111*, A09313, doi:10.1029/2006JA011763.

Luhmann, J. G. (1986), The solar wind interaction with Venus, *Space Sci. Rev.*, *44*, 241–306.

Luhmann, J. G., and L. H. Brace (1991), Near-Mars space, *Rev. Geophys.*, *29*, 121–140, doi:10.1029/91RG00066.

Lundin, R., L. Eliasson, B. Hultqvist, and K. Stasiewicz (1987), Plasma energization on auroral field lines as observed by the Viking spacecraft, *Geophys. Res. Lett.*, *14*, 443–446, doi:10.1029/GL014i004p00443.

Lundin, R., et al. (2006), Plasma acceleration above Martian magnetic anomalies, *Science*, *311*, 980–983, doi:10.1126/science.1122071.

Menietti, J. D., and J. L. Burch (1985), "Electron conic" signatures observed in the nightside auroral zone and over the polar cap, *J. Geophys. Res.*, *90*(A6), 5345–5353, doi:10.1029/JA090iA06p05345.

Menietti, J. D., and D. R. Weimer (1998), DE observations of electric field oscillations associated with an electron conic, *J. Geophys. Res.*, *103*(A1), 431–438, doi:10.1029/97JA02496.

Menietti, J. D., C. S. Lin, H. K. Wong, A. Bahnsen, and D. A. Gurnett (1992), Association of electron conical distributions with upper hybrid waves, *J. Geophys. Res.*, *97*(A2), 1353–1361, doi:10.1029/91JA02392.

Menietti, J. D., D. R. Weimer, M. Andre, and L. Eliasson (1994), DE1 and Viking observation associated with electron conical distributions, *J. Geophys. Res.*, *99*(A12), 23,673–23,684, doi:10.1029/94JA02133.

Mitchell, D. L., R. P. Lin, C. Mazelle, H. Reme, P. A. Cloutier, J. E. P. Connerney, M. H. Acuña, and N. F. Ness (2001), Probing Mars' crustal magnetic field and ionosphere with the MGS electron reflectometer, *J. Geophys. Res.*, *106*(E10), 23,419–23,427, doi:10.1029/2000JE001435.

Nagy, A. F., D. Winterhalter, and K. Sauer (2004), Plasma environment of Mars, *Space Sci. Rev.*, *111*, 33–114, doi:10.1023/B:SPAC.0000032718.47512.92.

Roth, I., M. K. Hudson, and M. Ternerin (1989), Generation models of electron conics, *J. Geophys. Res.*, *94*(A8), 10,095–10,102, doi:10.1029/JA094iA08p10095.

Soobiah, Y., et al. (2006), Observations of magnetic anomaly signatures in Mars Express ASPERA-3 ELS data, *Icarus*, *182*, 396–405, doi:10.1016/j.icarus.2005.10.034.

Temerin, M. A., and D. Cravens (1990), Production of electron conics by stochastic acceleration parallel to the magnetic field, *J. Geophys. Res.*, *95*(A4), 4285–4290, doi:10.1029/JA095iA04p04285.

Thompson, B., and R. L. Lysak (1994), Electron acceleration by the ionospheric Alfven resonator, in *Physics of Space Plasmas*, edited by T. Chang, p. 525, Scientific, Cambridge, Mass.

Ulusen, D., and I. Linscott (2008a), Transient events in the solar wind interaction of Mars due to the strong crustal fields, paper presented at Chapman Conference on the Solar Wind Interaction With Mars, AGU, San Diego, Calif.

Ulusen, D., and I. Linscott (2008b), Low energy electron current in the Martian tail due to reconnection of draped IMF and crustal magnetic fields, *J. Geophys. Res.*, *113*, E06001, doi:10.1029/2007JE002916.

Wong, H. K., J. D. Menietti, C. S. Lin, and J. L. Burch (1988), Generation of electron conical distributions by upper hybrid waves in the Earth's polar region, *J. Geophys. Res.*, *93*(A9), 10,025–10,028, doi:10.1029/JA093iA09p10025.

D. A. Brain, D. L. Mitchell, and D. Ulusen, Space Sciences Laboratory, University of California, Berkeley, CA 94720, USA. (demet@ssl.berkeley.edu)